

# Accretion states and radio loudness in Active Galactic Nuclei: analogies with X-ray binaries

Elmar G. Körding<sup>\*</sup>, Sebastian Jester<sup>†</sup>, Rob Fender

*School of Physics and Astronomy, University of Southampton, Southampton SO17 1BJ, United Kingdom*

Accepted 2006 August 17 Received 2006 August 17 in original form 2006 June 23

## ABSTRACT

Hardness-intensity diagrams (HIDs) have been used with great success to study the accretion states and their connection to radio jets in X-ray binaries (XRBs). The analogy between XRBs and active galactic nuclei (AGN) suggests that similar diagrams may help to understand and identify accretion states in AGN and their connection to radio loudness. We construct “disc-fraction luminosity diagrams” (DFLDs) as a generalization of HIDs, which plot the intensity against the fraction of the disc contribution in the overall spectral energy distribution (SED). Using a sample of 4963 Sloan Digital Sky Survey (SDSS) quasars with ROSAT matches, we show empirically that an AGN is more likely to have a high radio:optical flux ratio when it has a high total luminosity or a large non-thermal contribution to the SED. We find that one has to consider at least two-dimensional diagrams to understand the radio loudness of AGN. To extend our DFLD to lower luminosities we also include a sample of low-luminosity AGN. Using a simulated population of XRBs we show that stellar and supermassive BHs populate similar regions in the DFLD and show similar radio/jet properties. This supports the idea the AGN and XRBs have the same accretion states and associated jet properties.

**Key words:** accretion, accretion discs – black hole physics – galaxies:active – quasars:general – ISM: jets and outflows – X-rays:binaries

## 1 INTRODUCTION

In spite of a vast difference of scales, both black-hole X-ray binaries (XRBs) and active galactic nuclei (AGN) are thought to be powered by an essentially scale-invariant central engine consisting of a black hole, an accretion disc surrounded by a corona and a relativistic jet (e.g., Shakura & Sunyaev 1973; Antonucci 1993; Mirabel & Rodríguez 1999). In the study of AGN, it is a long-standing puzzle that some objects show strong radio emission while in others only little radio emission is found, even though their optical properties are similar (Kellermann et al. 1989; Miller et al. 1993). XRBs, i.e., stellar-mass accreting black holes, show states associated with strong radio emission as well as states during which the radio emission is strongly suppressed or “quenched” (Tananbaum et al. 1972; Fender et al. 1999; Corbel et al. 2000; Fender 2001). The different levels of radio emission have been ascribed to different jet properties of the different accretion states (e.g., Fender et al. 2004). Due to the shorter timescales of accretion onto XRBs, it is possible to study the

different accretion states and their association with jets in detail.

The quantitative comparison of XRBs and AGN has made a major step forwards in recent years with the discovery of a *fundamental plane of black-hole activity* (Merloni et al. 2003; Falcke et al. 2004). This is a correlation between radio and X-ray luminosities and black hole mass which fits both classes of objects (both individually and as an ensemble). Also the variability properties of AGN and XRBs show many similarities (Uttley et al. 2002; Markowitz et al. 2003; Körding & Falcke 2004; Abramowicz et al. 2004). Therefore, it is a promising route to use the concepts and methods developed to study the evolution of radio jets in XRBs for exploring the puzzle of the radio loudness in AGN.

XRB outbursts seem to occur in cycles of several distinct states that are similar in every large outburst and from object to object (e.g., Nowak 1995; Belloni et al. 2005, see Fig. 1). At the beginning of the cycle the source is in the *hard state* characterised by a hard power law in the X-ray spectrum. At radio frequencies, one usually observes a steady jet (Fender 2001). In this state the standard accretion disc (Shakura & Sunyaev 1973) is probably truncated or unobservable for some other reason and the inner

<sup>\*</sup> E-mail: Elmar@phys.soton.ac.uk

<sup>†</sup> Otto Hahn Fellow

part of the accretion disc replaced by an inefficient accretion flow (e.g., an advection dominated accretion flows, ADAF: Narayan & Yi 1994; Chen et al. 1995; Esin et al. 1997 but see also Miller et al. 2006). The X-rays are usually described with Comptonization models (e.g. Thorne & Price 1975; Sunyaev & Trümper 1979). However, it is also possible that the compact jet may contribute to the X-ray emission or even dominate it (Markoff et al. 2001, 2005). Once the source leaves the hard state, it is often found in an *intermediate state* (IMS). One finds two IMSs: first, the source enters a *hard IMS* characterised by a hard spectral component and band-limited noise in the power spectrum. Also in this state a jet is observed in the radio. Later, a *soft IMS* is found, dominated by a soft spectral component with power-law noise in the power spectrum (e.g., Belloni et al. 2005). Approximately at the transition from the soft to the hard IMS one usually finds a radio flare and the ejecta can often be resolved in the radio band. In the soft IMS no radio emission is found. After leaving the IMS, the source may go to the *soft state*, where the X-ray spectrum is dominated by a soft thermal component that is thought to originate from a standard accretion disc. The radio jet is still quenched in this state (Fender et al. 1999; Corbel et al. 2000).

It has not been established definitely how the phenomenology of AGN can be mapped onto these XRB states. Quasars are AGN with bright optical continuum emission, which are thought to have high accretion rates and strong disc emission (e.g., Urry & Padovani 1995). Here, we use the term AGN in a general sense to mean all supermassive accreting black holes, and we use the term “quasar” irrespective of the radio properties, i.e., synonymous with “quasi-stellar object” (QSO), and without imposing any luminosity cut.

For AGN, one commonly adopted definition of a “radio-loud” source is for the  $R$  parameter, the ratio of the radio flux (at 1.4 GHz) to the optical  $B$ -band flux, to be larger than 10. We follow this convention here. It has been known for over two decades that radio-loud quasars have higher X-ray fluxes than radio-quiet objects (e.g., Zamorani et al. 1981; Elvis et al. 1994; Zdziarski et al. 1995), perhaps hinting (with hindsight) that they represent different accretion states. Pounds et al. (1995) suggested that narrow-line Seyfert 1 objects may be analogues of the soft state. The fundamental plane of accreting black holes has been interpreted as evidence that low-luminosity AGN (LLAGN) are hard-state objects (Falcke et al. 2004; Körding et al. 2006). This has also been suggested by Ho (2005), based on the lack of an observable “big blue bump” in the spectral energy distributions (SEDs) of LLAGN. Again using the fundamental plane, Maccarone et al. (2003) suggested that AGN with an intermediate accretion rate (a few percent of the Eddington rate) are the analogue of soft-state XRBs.

On the other hand, Boroson (2002) has suggested that radio-loud and radio-quiet quasars occupy distinct regions of a two-dimensional diagram of physical accretion rate  $\dot{M}$  against Eddington-scaled luminosity  $L/L_{\text{Edd}}$ . Boroson considers these two quantities as the likely physical origin of the “eigenvectors” 1 and 2 (Boroson & Green 1992), and eigenvector 1 appears to be related to the radio properties. The division between radio-loud and radio-quiet objects proposed by Boroson (2002) is one in black-hole mass, similar to those reported elsewhere (Franceschini et al. 1998;

Lacy et al. 2001; Jarvis & McLure 2002). However, neither Ho (2002) nor Woo & Urry (2002) found any evidence for a mass threshold between radio-loud and radio-quiet objects. Thus, the physical mechanism making some sources much more radio-loud than others remains a puzzle.

For X-ray binaries, hardness-intensity diagrams (HIDs) have been used with great success to study the evolution of outbursts and separate the different accretion states (e.g. Homan et al. 2001; Fender et al. 2004; Belloni et al. 2005). The radio-loud and radio-quiet phases of a source are well separated on this HID. Additionally, the timing properties of the X-ray lightcurve change dramatically with the position in the HID (e.g., Homan et al. 2001; Belloni et al. 2005; Remillard 2005). Hence, the construction of equivalent diagrams promises to be a useful tool for the study of AGN, too. For XRBs, X-ray HIDs are useful diagnostic tools because spectral features of both the accretion disc and the hard power-law component are visible in the X-rays. The black-body temperature of the accretion disc scales with black hole mass as  $M^{-1/4}$  so that the SEDs of accretion discs around supermassive black holes peak in the optical/ultra-violet and an X-ray HID for AGN would not contain any information about the disc emission. Therefore, we have to construct a new type of diagram which is applicable to the study of XRBs as well as of AGN. In this paper, we present the definition of an analogous diagram for AGN (§2) and use our method to explore the origin of radio loudness in a sample of quasars from the Sloan Digital Sky Survey (SDSS) and LLAGN (§3), also considering the impact of selection effects and other biases (§4). We compare the behaviour of AGN and X-ray binaries in §5 and conclude in §6.

## 2 METHOD

### 2.1 Scaling hardness flux diagrams from XRBs to AGN

X-ray HIDs are used to study the evolution of an XRB during an outburst (Fender et al. 2004; Belloni et al. 2005). On the ordinate ( $y$ -axis) of these diagrams, one usually plots the X-ray count rate, while the abscissa ( $x$ -axis) denotes the hardness ratio (e.g., 6.3–10.5 keV count rate/3.8–6.3 keV count rate). For a sketch of a typical HID see Fig. 1. While a source is in the *hard state*, its hard power-law, generally assumed to arise via Comptonization, dominates the spectrum and the source is on the right-hand (hard) side of the diagram. The X-ray emission in the *soft thermally-dominated state* is believed to be mainly due to a standard thin accretion disc (multi-temperature black-body). In this state, the source moves towards the left of the diagram. In AGN, the thermal emission of the accretion disc peaks in the optical or ultra-violet — far from the observed X-ray bands. Thus, an HID based solely on the X-ray spectrum cannot probe whether an AGN is in a “soft” or “hard” state.

An HID that can be used to diagnose AGN as well as XRBs has to be based on parameters that are independent of the observing band, as at least the temperature of the accretion disc and therefore the peak of the emission component scales with black hole mass. The location of an individual source in the HID is determined by the total luminosity of the system and the relative strength of the power law

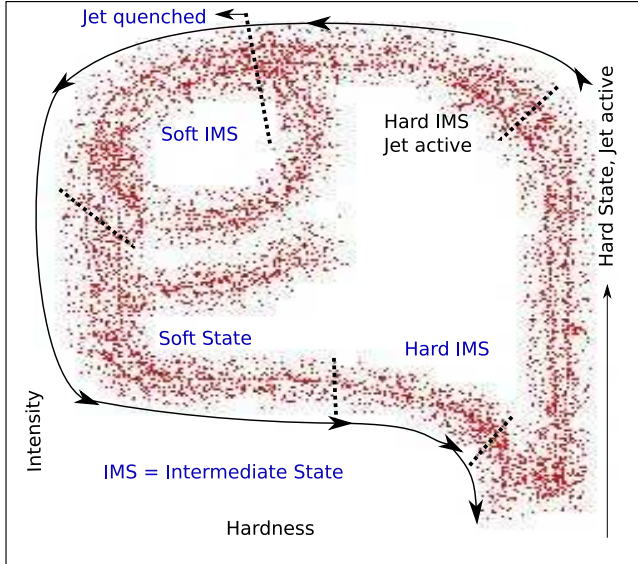


**Figure 1.** Sketch of an HID found for XRBs. For the abscissa one usually uses the hardness ratio and the ordinate represents the measured X-ray counts, i.e., the total measured X-ray flux. The arrows indicate the movement of a source during outburst.

component compared to the disc component of a source. In XRBs, both the disc and the power-law component are observable in the X-ray band. The *X-ray luminosity* is (caveat bolometric corrections) equal to the luminosity  $L_D + L_{PL}$ , where  $L_D$  denotes the disc luminosity and  $L_{PL}$  the luminosity of the power-law component. The *hardness* reflects which component dominates the spectrum. Thus,  $\frac{L_{PL}}{L_D + L_{PL}}$  has a similar behaviour as the hardness ratio. We will refer to this quantity as the *non-thermal fraction*. This value approaches zero for disc-dominated sources and 1 if the power law is the dominating component.

In AGN, the disc luminosity can be measured in the optical band for non-obscured sources, while X-ray observations provide information only about the power-law component. A benefit of the term  $\frac{L_{PL}}{L_D + L_{PL}}$  is that it stays finite if one of the components approaches zero, which happens when a source is in the hard or the soft state. As it is a ratio of luminosities, it is furthermore independent of the distance. For the case that the luminosities of both spectral components scale similarly with BH mass, it is also independent of the BH mass. We will refer to diagrams plotting  $L_D + L_{PL}$  against  $\frac{L_{PL}}{L_D + L_{PL}}$  as *disc-fraction/luminosity diagrams* (DFLDs).

We note in passing that the ratio  $\frac{L_{PL}}{L_D + L_{PL}}$  is probably connected to the properties of the accretion disk wind at least in AGN. The UV luminosity ( $L_D$ ) is a measure of the radiation pressure while the X-ray luminosity ( $L_{PL}$ ) influences the ionisation state (see, e.g., Richards 2006, and references therein).

For XRBs we can observe the evolution of an entire outburst of an individual source and obtain a closed loop on the HID or DFLD, as the timescales of an outburst is months to years (Chen et al. 1997). For each position in the diagram we can observe whether or not the jet is visible. However, for AGN it is impossible to observe a full outburst cycle (quiescent  $\rightarrow$  quasar phase  $\rightarrow$  quiescent) as it would last for

hundreds of millions of years (assuming a linear scaling of timescales with BH mass). Instead, we have to study a large population of AGN in the DFLD and observe their average radio loudness (i.e., the radio:optical flux ratio) as a tracer of the jet activity.

## 2.2 Our sample

To construct a DFLD for AGN we need a sample of AGN with well measured optical ( $L_D$ ), X-ray ( $L_{PL}$ ) and radio fluxes.

### 2.2.1 SDSS Quasars

As our main sample, we begin with the lists of all objects from the spectroscopic database<sup>1</sup> of SDSS DR5 (J. Adelman-McCarthy et al., *in prep.*; Adelman-McCarthy et al. 2006) that have been identified as a quasar with high confidence. The sample includes all objects from the statistically complete quasar survey (Richards et al. 2002) as well as quasar spectra selected in other ways, e.g., candidate optical counterparts of known X-ray sources (Anderson et al. 2003). Given the criteria used by the SDSS to classify objects as quasars, all objects are Type 1 quasars with strong broad emission lines (and potentially broad absorption lines). Appendix A gives the SQL query necessary to reproduce our initial sample. For X-ray and radio measurements, we use data from the ROSAT All-Sky Survey (RASS, energy band 0.1–2.4 keV; Voges et al. 1999) and the Very Large Array (VLA) Faint Images of the Radio Sky at Twenty centimeters (FIRST) survey (White et al. 1997, observing frequency 1.4 GHz;) as given in the SDSS database. The radio fluxes are intended to be a measure of the core radio flux of our sources (see §4.4). We only include quasars in the redshift range  $0.2 \leq z \leq 2.5$ . Below a redshift of 0.2, not many quasars are found, and spectra of low-luminosity AGN are often dominated by galaxy light, making them more likely to be classified as galaxy by the SDSS pipeline. Redshifts above 2.5 contribute only a small fraction of the total number of SDSS quasars, and not many of them have a ROSAT detection at such high redshifts. In the adopted redshift range, there are a total of 64248 objects of which 5174 have a radio detection, 4963 have an X-ray detection, and 730 have detections in both bands.

We apply a *K*-correction to the flux measurements in all three wavebands in order to remove apparent luminosity differences that are caused by observing objects at different redshifts, and therefore at different rest wavelengths. The *K*-correction is conventionally defined as  $m_{\text{intrinsic}} = m_{\text{observed}} - K(z)$  (see Hogg et al. 2002, e.g.). For the SDSS quasars, we use reddening-corrected *i*-band PSF magnitudes (identical to those used to flux-limit the SDSS main quasar sample) and apply the *i*-band *K*-correction given by Richards et al. (2006, Table 4). These authors remove the average contribution of emission lines as function of redshift to obtain a pure continuum luminosity with an assumed power-law spectrum  $f_\nu \propto \nu^{-0.5}$  and define the correction to

<sup>1</sup> <http://cas.sdss.org/astro>

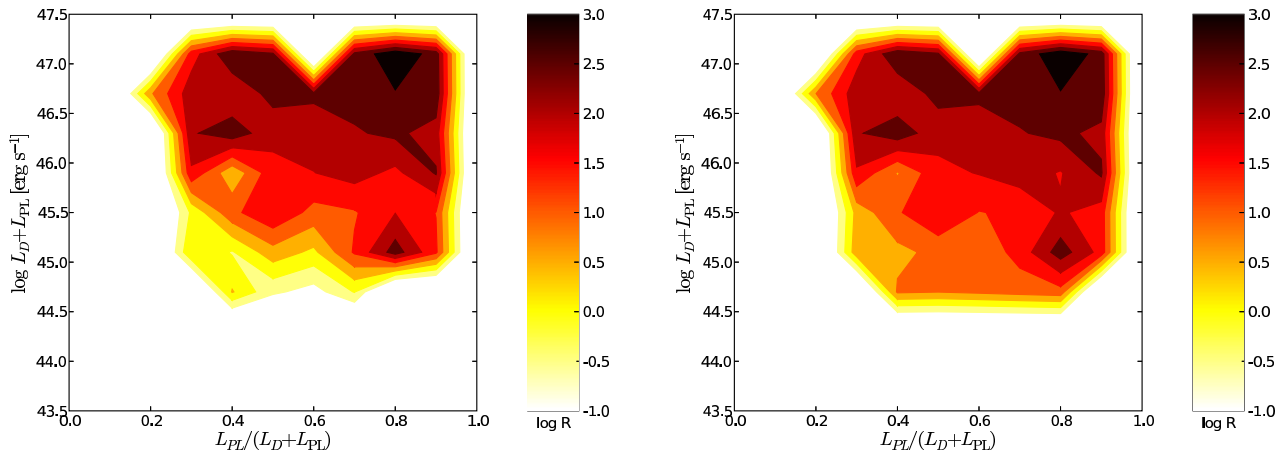


**Figure 2.** Left: DFLD of 4963 SDSS quasars with ROSAT detections in the redshift range  $0.2 \leq z \leq 2.5$ , showing the lower limit to the average radio loudness  $R$  as calculated from FIRST data. The contour levels are separated by 0.5 dex in  $R$ . Right: Upper limit to the average  $R$ . The contour levels are the same as for the lower limit.

be 0 at  $z = 2$ . The continuum  $K$ -correction is easy to compute since the SDSS magnitude system is (nearly<sup>2</sup>) an AB system (defined as  $\text{mag} = -2.5 \log(f_\nu / 3631 \text{ Jy})$  for a source with constant  $f_\nu$  Oke & Gunn 1983; Abazajian et al. 2003); the correction is given by  $K(z) = -2.5(1 + \alpha) \log(1 + z)$  for  $f_\nu \propto \nu^\alpha$ . We convert the  $K$ -correction to  $M_i(z = 2)$  back to the conventional  $M_i(z = 0)$  by adding the offset 0.596 appropriate for an object at redshift  $z = 2$  with the assumed power-law spectrum with  $\alpha = -0.5$  (see Richards et al. 2006, eqn. [1]). We then transform to the  $B$ -band using  $B - i = 0.3$  as appropriate for the same power-law spectrum. Thus, the  $B$ -band magnitude is obtained from the SDSS  $i$ -band PSF magnitude, galactic extinction  $A_i$  as given in the SDSS database, and the combined emission-line and continuum  $K$ -correction  $K_{\text{opt}}$  as

$$B = i + 0.3 - A_i - K_{\text{opt}} + 0.596. \quad (1)$$

However, we do not apply any correction for contributions from host galaxy starlight. This correction is most important for the lowest quasar luminosities and for the lowest-redshift objects. We discuss the impact of this simplification in §4.3.

For the  $K$ -correction of the radio fluxes we assume optically thin spectra with a spectral shape  $f_\nu \propto \nu^{-0.5}$ , i.e., we assume the same spectral shape for the radio and optical continua. For the X-ray data, we assume a photon index  $\Gamma = 2$ , i.e., a spectral shape  $f_\nu \propto \nu^{-1}$  (found to be appropriate for both radio-loud and radio-quiet quasars by Galbiati et al. 2005) which has 0  $K$ -correction because the effects of bandwidth narrowing and observing a steep spectrum at lower rest-frame frequencies cancel.

As the SDSS quasar sample includes objects with a large range of black-hole masses, it is in principle necessary to apply a mass correction to the observed luminosities. Accreting black holes that are observed as a quasar all have similar Eddington ratios, in the range 0.05–1 (e.g., Jester 2005). Hence, to zeroth order, the luminosity of a quasar is expected to scale as the Eddington luminosity, i.e., linearly with black

hole mass. However, the black hole masses computed for 12245 quasars from SDSS DR1 by McLure & Dunlop (2004) have a mean of  $(4.75 \pm 0.44) \times 10^8 M_\odot$ , i.e., the intrinsic scatter in the black hole mass of quasars accessible to the SDSS spectroscopic survey is comparable to the scatter in the black-hole mass determination (estimated to be as large as 0.5–0.6 dex by Vestergaard 2004). Hence, the black-hole masses of all SDSS quasars are consistent with being equal to the mean and we apply no mass scaling. This needs to be borne in mind when comparing this quasar sample to AGN samples with substantially different black hole masses.

We use a cosmology with  $\Omega_M = 0.3$ ,  $\Omega_\Lambda = 0.7$ ,  $H_0 = 71 \text{ km s}^{-1} \text{ Mpc}^{-1}$ .

### 2.2.2 Low-luminosity sample

While our main results will be based on the SDSS quasars, we construct a low-luminosity sample based on the sample of Ho et al. (1997) as a comparison. We have obtained X-ray fluxes for this sample from Terashima & Wilson (2003) and the following surveys in order of preference: The Chandra v3 pipeline (Ptak & Griffiths 2003<sup>3</sup>), the XMM serendipitous X-ray survey (Barcons et al. 2002), and the ROSAT HRI pointed catalog (ROSAT Scientific Team 2000). Radio fluxes for the sample have been taken from Nagar et al. (2005). For low-luminosity AGN, the optical emission is often dominated by galaxy light. Therefore, we use a correlation between  $H\beta$  and the  $B$ -band magnitude (Ho & Peng 2001):

$$\log L_{H\beta} = -0.34M_B + 35.1 \quad (2)$$

to compute the optical absolute magnitude. This correlation seems to hold for quasars as well as Seyfert galaxies. We use the correlation also for our low-ionization nuclear emission region (LINER) objects even though the correlation has only been shown to hold for Seyfert objects and PG quasars.

<sup>2</sup> See the discussion at <http://www.sdss.org/dr5/algorithms/fluxcal.html> and <http://www.xassist.org>

The average BH mass of the SDSS quasars is significantly larger than that of the nearby LLAGN. Thus, for LLAGN it is important to consider their BH masses. The BH masses of the LLAGN sample are calculated from the  $M$ - $\sigma$  relation (Merritt & Ferrarese 2001) using velocity dispersions from the Hypercat catalog (Prugniel et al. 1998). We scale the luminosities linearly with mass to the average mass of the SDSS quasars.

### 2.3 Calculating the component luminosities

To compute the accretion-disc luminosity, we use the relation between the absolute optical  $B$ -band magnitude and the approximate disc luminosity given by Falcke et al. (1995):

$$\log L_D = -0.4M_B + 35.9 \quad (3)$$

This disc luminosity measure has a scatter of 0.29 dex.

The power-law component  $L_{PL}$  is estimated from the X-ray luminosity. To obtain the power-law luminosity, we extrapolate the measured ROSAT counts to a flux in the 0.5-10 keV band using a photon index of  $\Gamma = 2$ . For the hydrogen column density we use an average Galactic column density of  $n_H \sim 1 \times 10^{21} \text{ cm}^{-2}$  (e.g., Dickey & Lockman 1990). The hydrogen column density in the Quasar is usually negligible of broad line Quasars (for the low absorption of broad line objects see, e.g., Richards et al. 2003), additionally, the large redshift reduces its effect. This yields a conversion factor of 1 cps  $\hat{=}$   $3.1 \times 10^{-11} \text{ erg s}^{-1} \text{ cm}^{-2}$ . Where Chandra observations are available, we can measure the flux in this energy range directly. The luminosity of the power-law component is chosen to be

$$L_{PL} = 3L_{0.5-10\text{keV}} \quad (4)$$

This ‘‘bolometric correction’’ of a factor 3 is fairly arbitrary and was chosen to distribute the quasars uniformly over the  $x$ -axis of the DFLD. For the purpose of our analysis, it does not have to correspond directly to the real bolometric correction of the quasar, but is probably not far off. However, a different value creates only a slightly different mapping of the sources on the defined axis. This is similar to the definition of the hardness ratio in the HIDs, which is also arbitrary and chosen to give a good distribution of the sources in the HID. Combining these ‘‘bolometric’’ and the  $K$ -corrections from §2.2.1 into the factors  $c_{\text{opt}}$  and  $c_X$ , our non-thermal fraction is related to the observed fluxes in both wavebands by  $1/(1 + c_{\text{opt}}f_{\text{opt}}/[c_X f_X])$ .

To compare the radio loudness of the AGN as function of their position in the DFLD, we also calculate the parameter  $R$ , which is defined as the ratio of the radio flux at 1.4 GHz divided by optical  $B$ -band flux. For inclusion in this diagram, we only accept sources which have optical and X-ray fluxes, but we include sources with only an upper limit for  $R$ . Including the expressions for our  $K$ -correction terms from §2.2.1,  $R$  is related to fluxes from the catalogues by the expression

$$\log R = 0.4(B - t) \quad (5)$$

(Ivezić et al. 2002), where  $t$  is the  $K$ -corrected 1.4 GHz radio AB magnitude given by  $t = -2.5[\log(f_{\text{FIRST}}/3631 \text{ Jy}) + 0.5 \log(1 + z)]$  and  $B$  is the  $K$ -corrected  $B$ -band magnitude from eqn. (1).

## 3 RESULTS

We can now use our samples of AGN to construct DFLDs, i.e., the  $y$ -axis of this diagram denotes  $L_D + L_{PL}$ , while on the  $x$ -axis we plot  $\frac{L_{PL}}{L_D + L_{PL}}$ . For every source, we can calculate the position in the DFLD and its radio loudness  $R$ , or an upper limit to  $R$ . To study the dependence of radio loudness on location in the DFLD, we compute the average radio loudness of AGN at each position. We do so by binning the data in  $10 \times 10$  cells of the DFLD and calculating the arithmetic mean of  $R$  for each cell. We only show those cells in the diagram that contain more than 10 sources. We treat the upper limits to  $R$  in two ways: First we set  $R$  to zero for all sources without a radio detection. This average  $R_{\text{low}}$  is a lower limit to the real average of  $R$ . Secondly, we set  $R$  to the upper limit of the corresponding radio measurement. This average,  $R_{\text{high}}$ , is an upper limit to the real average  $R$ . Thus, the real average  $R$  has to lie between these two values. We will use these values in our figures to detect selection effects caused by the FIRST survey’s radio flux limit.

### 3.1 SDSS Quasars

In Fig. 2 we show both upper and lower limit of the average  $R$  for our 4963 SDSS quasars with ROSAT detections. The average  $R$  value is largest in the upper right corner and declines gradually towards the lower left corner. The average  $\log R$  in the top right corner is 2.6 dex higher than in the bottom left corner, which corresponds to a factor 398 in  $R$ . The gradient is seen both in the upper and lower limit of  $R$  and the difference between both maps is very small. Thus, we conclude that this effect is also found in the real averaged  $R$ . The effect can be described as combination of two trends: First, the most radio-loud objects for a given disc luminosity (i.e., optical luminosity) are among those sources that are the most X-ray bright (see Fig. 3). Additionally, brighter objects tend to be more radio-loud for a given disc fraction (a fixed  $x$ -value in the DFLD). The first effect is already known as radio-loud objects are known to be more X-ray bright (e.g., Elvis et al. 1994; Shen et al. 2006).

As the average has been computed separately for every cell, two different cells are statistically independent. Thus, even though the average in each cell does not have to be significant, the fact that the map is smooth and has a well-defined gradient in  $R$  indicates that this effect is not a statistical artifact. To verify this observation mathematically, we have performed a Kolmogorov-Smirnov test of the differences between the distributions of radio loudness in two well-separated areas of the DFLD. We compare all sources within a ‘‘high-luminosity’’ area given by  $0.3 \leq x \leq 0.5$  and  $46 \leq y \leq 47$  to those in a ‘‘low-luminosity’’ area given by  $0.3 \leq x \leq 0.5$  and  $44 \leq y \leq 45.5$ . In Fig. 4 we show the  $\text{Log } N - \text{Log } R$  diagrams for both areas. Already visual inspection suggests that the ‘‘high-luminosity’’ area contains a significantly larger fraction of radio-loud objects. This is confirmed by the Kolmogorov-Smirnov test, which rules out that the two underlying probability distributions are identical with a confidence level of 99.994 % ( $D = 0.19$ ). We also verified that the radio-loudness distribution is different for areas with similar luminosity but different disc-to-power law ratios.

To verify that the X-ray emission does have an effect on

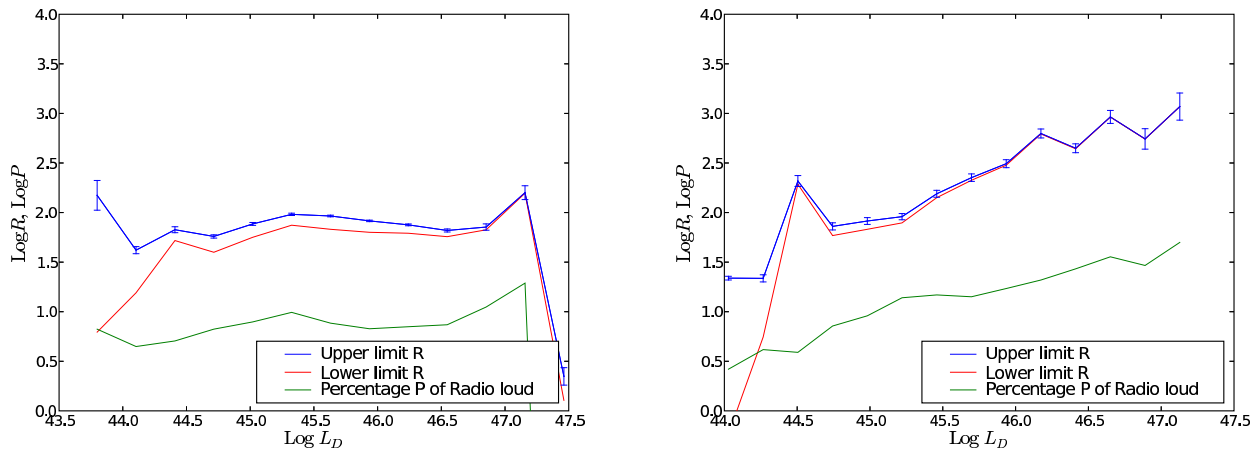


**Figure 5.** Limits to average radio loudness and percentage of radio-loud sources ( $R > 10$ ) as function of disc luminosity. Left: all 64248 SDSS quasars in the redshift range  $0.2 \leq z \leq 2.5$ . Right: only the 4963 X-ray detected sources. The error bars give the uncertainty of the mean in each of the bins.

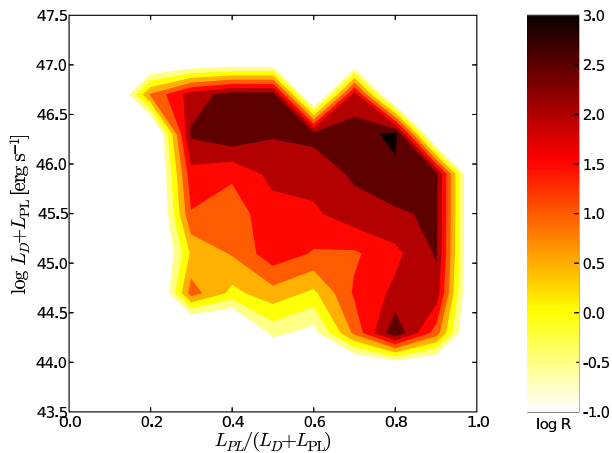


**Figure 3.** Modified DFLD showing the average radio-loudness. The y-axis gives the optical disc luminosity  $L_D$  instead of the sum of the disc and the power law luminosity in the previous maps. The most radio-loud sources are those with a large power law component in the spectrum.

the radio loudness, we plot the average radio loudness as a function of the disc luminosity (i.e., the optical luminosity) in the left-hand panel of Fig. 5, for all 64248 SDSS objects, independently of their X-ray detection. The average  $R$  has been estimated independently in 20 logarithmic luminosity bins. This plot of the radio loudness as a function of luminosity can be compared to the right-hand panel of the same figure, where we show the dependence of the radio loudness on the disc luminosity for the 4963 X-ray detected sources only. While there is the clear trend visible in the X-ray detected quasars that brighter objects are more radio-loud, only marginal effects can be seen in the full sample. We show the upper and lower limit to the radio loudness as well as the fraction of radio-loud objects as defined by  $R > 10$ . The trend can be seen in all three quantities. We can also find a clear trend in the radio-loudness if we project the

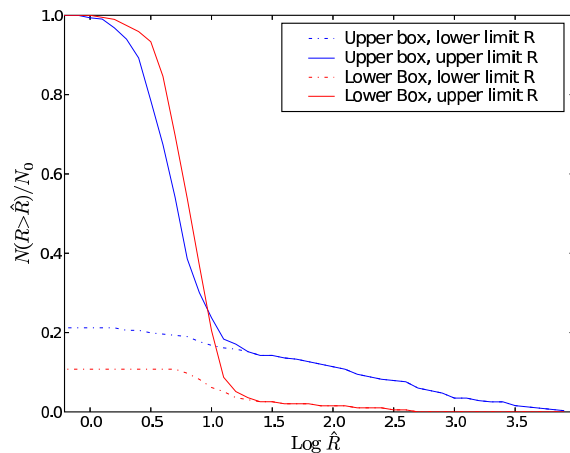


**Figure 4.** Log  $N$ -log  $R$  diagram for two rectangular areas in the DFLD diagram. The position and extent of the upper and lower box is given in the text. For both areas we first find all objects with a position on the DFLD in that area and construct log  $N$ -log  $R$  diagrams for both areas individually. Solid lines indicate upper limits to the average  $R$  while dashed lines represent its lower limit.

DFLD onto an axis roughly corresponding to the diagonal. In Fig. 6 we show such a projection for the SDSS sample (compare Shen et al. 2006, Fig. 11).

### 3.2 Hard-state objects: LLAGN

So far, we have only considered the SDSS quasars. All quasars are thought to be strongly accreting objects with a standard geometrically thin, optically thick disc. To obtain information about the shape of the DFLD at lower luminosities, which may be in a different, radiatively inefficient accretion mode, we now include the sample of Ho et al. (1997). Due to the small number of sources we now show every cell for this sample, even if it includes only one source. Hence, for the LLAGN, the plotted “mean”  $R$  may just be a single

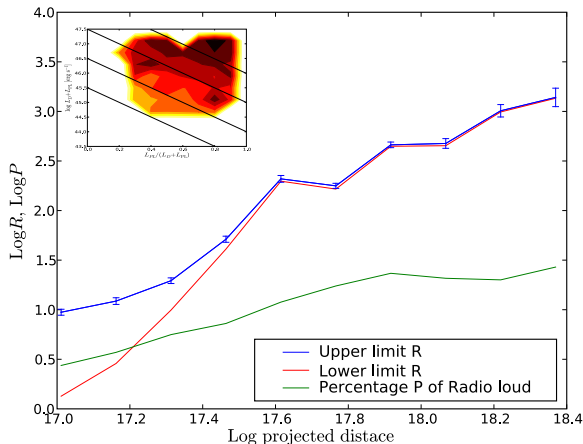


**Figure 6.** Projection parallel to the black lines in the DFLD shown in the inset (with the chosen scaling of the coordinate axes, the line *onto* which objects are projected is not perpendicular to these lines). We project on to the line defined by  $\lambda = (0.93 e_x + 0.36 e_y)$ . This projection includes only sources with measured X-ray fluxes.

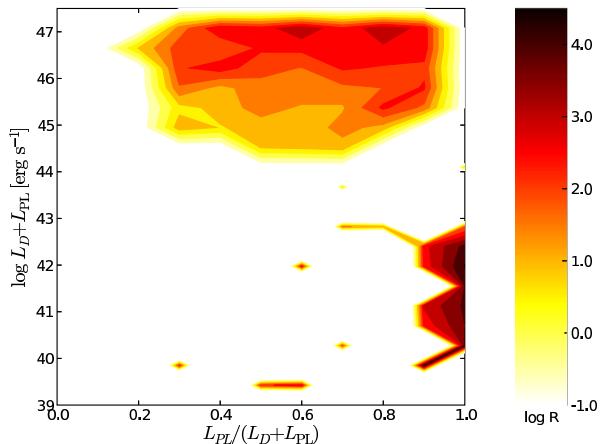


**Figure 7.** DFLD showing the average radio loudness for SDSS quasars and LLAGN from the Ho (1999) sample. Note that the gap between LLAGN and Quasars is an artefact of our sample selection.

measurement that could be substantially different from the true mean  $R$ .

In Fig. 7 we show the joint DFLD for the SDSS quasars and the LLAGN sample. Not surprisingly, the LLAGN lie at lower luminosities than the SDSS quasars. However, except for a few outliers they all lie at the right side of the DFLD. This is also not surprising, as Ho (1999) already noted that LLAGN are less optically bright for a given X-ray luminosity than strongly accreting AGN (Seyfert galaxies and quasars). Furthermore, the LLAGN in our DFLD seem to be more radio-loud on average than SDSS quasars. As mentioned, we have to plot every cell for the LLAGN even if it only contains one object, so the mean value of  $R$  for any given cell may not be close to the true mean. But already Ho & Peng (2001)

have shown that the average low-luminosity Seyfert galaxy is more radio-loud than the average “radio-loud” PG quasar if only the nuclear luminosity is considered (i.e., removing the contribution of starlight). Thus, we find that LLAGN populate the bottom right-hand side of the DFLD and are — on average — more radio-loud than the SDSS quasars.

## 4 CRITICAL ANALYSIS OF SELECTION EFFECTS AND ASTROPHYSICAL BIASES

In this section, we consider whether the shape of the distribution of SDSS quasars in the DFLD and their average radio loudness could be caused entirely due to selection effects, or underlying correlations between the observables and other parameters. We consider in detail the selection effects of flux-limited samples (§4.1), black-hole mass scalings (§4.2), orientation, beaming and host-galaxy light (§4.3) and the size-luminosity evolution of radio sources (§4.4). Based on our analysis, none of these effects can produce the entire signal we report.

### 4.1 Selection effects

Our main sample is basically a single quasar survey with a fairly bright flux limit — most quasars in our sample are drawn from that part of the quasar sample limited by  $i < 19.1$ . Even though we include several other SDSS target categories, there is an implicit flux limit  $i \lesssim 20$  imposed by the signal-to-noise that can be achieved in the exposure time of the spectroscopic observations in the SDSS. As the optical luminosity function of quasars is rather steep, this means that the dominant selection effect is that we only have a rather restricted dynamic range in quasar luminosity at fixed redshift, of order 10–30 (the SDSS spectroscopic survey has a bright limit  $i > 15$  and substantial numbers of objects are only found at  $i \gtrsim 16$ ). Thus, only the most luminous object at any given redshift are found, and the variation in luminosity is largely due to a variation in redshift. Thus, on average there is a clear trend that the redshift of the lowest luminosity sources is small ( $z = 0.2$ ) while the highest luminosities are found at large distances ( $z = 2.5$ ).

To assess the impact of this well-known degeneracy between redshift and luminosity in flux-limited surveys, we have verified that the effect is visible in small redshift slices, e.g., in the subsample with redshifts between  $z = 0.3$  and  $z = 0.4$  as shown in Fig. 8. Furthermore, we have verified that the  $K$ -correction is not creating the observed trends in the DFLD. Even if we assume a flat radio spectrum or do not  $K$ -correct at all, we find the observed effect. The difference in radio loudness between the average SDSS quasar at low redshift ( $z \approx 0.2$ ) and those at large redshifts ( $z \approx 2.5$ ) is 0.6 in  $\log R$ . This difference is probably mainly due to a difference in accretion rates. However, even if this is purely due to evolution, we note that the observed range in  $R$  in the DFLD is around 2.5 dex, so evolution would only be a minor effect. This suggests that the radio loudness gradient in the DFLD is not an artifact of redshift evolution, but we cannot rule out that evolution plays a minor role. It clearly will be desirable to construct a DFLD with a sample that is not affected by evolution (i.e., one with a narrow redshift distribution).

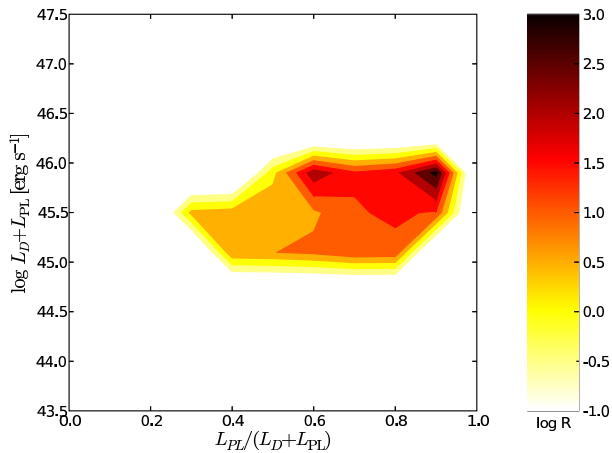


**Figure 8.** DFLD of the redshift slice  $0.3 \leq z \leq 0.4$ . In this redshift range our sample contains 676 sources with optical and X-ray detections of which 70 also have radio detections. Due to the small number of available sources we show all bins with more than 5 sources. Similar to the DFLD of the full sample sources in the upper right corner have large average  $R$  values, while those in the lower left are less radio-loud.

We have shown the average radio loudness as a function of the position in the DFLD in two versions: as an upper limit and as a lower limit to the real radio loudness (i.e., the value we would observe with a radio telescope of infinite sensitivity). More sensitive radio observations would increase the lower limits while they would decrease the upper limit map. As there are only minor differences between both maps, we conclude that our result is not affected strongly by the radio detection limit.

As an additional test, we have performed a Monte-Carlo simulation to check whether the trends observed in the DFLD for the SDSS quasars are merely due to selection effects arising from the use of flux-limited surveys. As null hypothesis, we assume that radio, optical and X-ray fluxes of all objects are uncorrelated, so that the conditional luminosity function is simply the product of the individual luminosity functions:  $\Phi(L_R, L_O, L_X) = \Phi_1(L_R) \Phi_2(L_O) \Phi_3(L_X)$ . At the high luminosities that are accessible to our three surveys, all three luminosity functions are well-described by simple power laws  $\Phi(L) \propto L^{\beta_{R,O,X}}$ . For the radio luminosity function we use  $\beta_R = 0.78$  (Nagar et al. 2005), for the X-rays  $\beta_X = 2.34$  (Ueda et al. 2003) and for the optical luminosity function  $\beta_O = 2.95$  (Richards et al. 2006). For this simple test we assume that the power law indices do not change with redshift. The number of sources with radio, optical and X-ray detections at a given redshift is fixed to the observed value. This incorporates density or luminosity evolution with redshift, as well as the redshift-dependent selection efficiency of the SDSS quasar survey. The resulting DFLD of the simulated sample is shown in Fig. 9. The trend visible in the observed DFLD (Fig. 2), i.e., an increase in the mean radio loudness from the bottom left to the top right, is not observed. Furthermore, we have repeated this luminosity function test with a population of artificially beamed steep-spectrum sources: a population of steep-spectrum sources with  $\beta_R = 2.31$  (Willott et al. 2001), 10% of which have

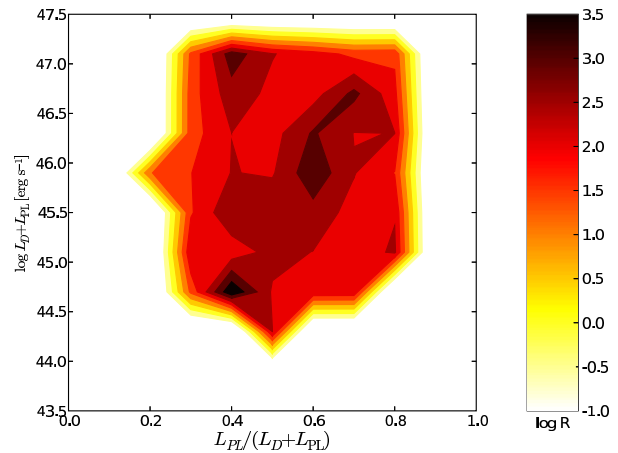


**Figure 9.** Monte-Carlo simulation of the radio loudness as a function of the position on the DFLD, assuming no correlation between radio, optical and X-ray luminosities. We assume simple power-law luminosity functions and give the simulated sample the same redshift distribution as our observed sample.

their radio flux increased by a factor 100, but still without correlation to optical or X-ray properties. This simulation cannot reproduce our findings, either.

## 4.2 Black-hole mass

We are not able to correct the DFLD of our SDSS quasars for the BH mass as we do not know the mass for most of our objects. Even though most quasars in the SDSS have masses around  $8.7 \times 10^8 M_\odot$  (McLure & Dunlop 2004), more luminous objects are more likely to have a more massive black hole. Thus, objects in the lower-luminosity part of the diagram will have a lower mass on average, while high-luminosity objects will have larger BHs. It has been suggested that the radio power of AGN correlates with BH mass (Franceschini et al. 1998; Lacy et al. 2001; Jarvis & McLure 2002). Also the fundamental plane of black-hole activity (Merloni et al. 2003; Falcke et al. 2004) suggests a weak mass dependence as the radio luminosity depends nonlinearly on the accretion rate (not scaled to Eddington units). However, other researchers have found no evidence for correlations between radio loudness or radio power and black-hole mass (see Ho 2002; Woo & Urry 2002, e.g.), as selection effects severely affect most of the studied samples. Thus, it is important to explore whether a mass dependence of the radio loudness can modify our findings.

In the left-hand panel of Fig. 5, we plot the average radio loudness against disc luminosity, i.e., the optical luminosity. We do not find a strong correlation between the two as long as we consider all SDSS quasars. Only when we exclude X-ray non-detections, a clearer trend is found. But also in the first plot the most luminous objects should have — on average — larger BH masses than the faint objects. Thus, a strong mass effect is not seen for all SDSS quasars with radio detections. Furthermore, it is well-known that radio-loud objects are more X-ray bright (e.g., Elvis et al. 1994). This supports the idea that the observed dependence



of radio loudness on position in the DFLD is not purely due to different black hole masses.

Jet models often assume a linear coupling between the accretion power and the power injected into the jet (e.g., Falcke & Biermann 1995; Meier 2001). This suggests that larger black holes should have larger radio luminosities as the physical accretion rate is higher for a fixed Eddington ratio. In our DFLD we show the radio loudness, i.e. the ratio of the radio flux and the flux in the  $B$ -band. A constant  $R$  indicates that the radio flux scales linearly with optical flux and probably the accretion rate. However, it may be that the radio luminosity scales with a higher power of the accretion rate. E.g., for the radio core, the radio luminosity scales roughly with  $L_{Rad} \propto \dot{M}^{1.4}$  if the jet power is a constant fraction of the accretion rate (Blandford & Königl 1979). This scaling is further supported by the “fundamental plane of accreting black holes” (Falcke et al. 2004; Merloni et al. 2003; Körtling et al. 2006). We have verified that this effect does not change the plot of the radio-loudness in the DFLD. The figure looks similar if we plot  $L_{Rad}/L_D^{1.4}$  (this assumes that the disc luminosity is a good tracer of  $\dot{M}$ ). Thus, this dependence of the radio luminosity on accretion rate cannot reproduce the observed diagrams.

It has been suggested that instead of a *correlation* between  $R$  and black-hole mass, there is a hard switch in radio loudness for source with BH masses  $M > 10^8 M_\odot$  (e.g., Laor 2000; McLure & Jarvis 2004). The Eddington limit for a  $10^8 M_\odot$  BH is around  $10^{46}$  erg s $^{-1}$ , but our DFLD still shows a gradient in radio loudness above this luminosity. This gradient can therefore not be solely due to a single switch. Thus, if the BH mass is the dominant effect in the DFLD, there must be an additional mass dependence besides the suggested switch around  $M > 10^8 M_\odot$ .

As a “worst-case scenario”, let us assume that all objects have a fixed Eddington ratio. In this case, the luminosity range of 2 orders of magnitude is due to 2 orders of magnitude difference in the black-hole mass. The highest and lowest average values of  $R$  found in our DFLD differ by a factor  $10^{2.3}$ . If the differences in radio loudness were purely due to a mass dependence, this would suggest that  $L_R \propto M^{2.3}$ . Furthermore, if this effect was to explain the entire radio-loudness distribution on the DFLD, the most massive black holes would have to be the most X-ray bright objects (i.e., lie on the right-hand side of the diagram). This does not seem to be the case (e.g., Woo et al. 2005). Since the required mass scaling seems to be rather large (compare Fig. 2 in McLure & Jarvis 2004) and the needed X-ray to optical properties are not found, we consider it unlikely that the radio loudness distribution in the DFLD arises purely due to a mass scaling of the radio loudness.

### 4.3 Orientation, beaming, and host galaxy light

The orientation of a quasar’s accretion disc and jet with respect to the observer can play an important role for the observed luminosities (see e.g., Urry & Padovani 1995). The main effects are relativistic beaming of the emission originating from the jet and obscuration of disc and broad-line emission by a torus. All our SDSS quasars are of Type 1, so broad lines are visible in all objects. It follows that we select only sources that are not strongly obscured (see also the discussion of the likely fraction of reddened quasars in the

SDSS by Richards et al. 2003; Hopkins et al. 2004). This is especially important as we use soft X-ray data from ROSAT, which is very sensitive to absorption. Due to our selection of broad-line objects, we ensure that the emission lines are not swamped by the featureless continuum of the relativistic jet (a BL Lac object would not be classified as a broad-line SDSS quasar). Hence, we are selecting against strongly boosted sources.

Thus, we can safely assume that the optical emission is mostly due to the accretion disc. Radio emission, however, is known to be strongly affected by beaming, because it arises from a relativistic jet. If radio emission is the only beamed component in the SED, any correlation between the strength of the beaming and the position of the source in the DFLD supports our statement that the jet properties of AGN depend on both the optical and X-ray properties of the source.

In case that some or all of the X-ray emission also originates from the jet, the X-ray bright sources on the right side of the DFLD will preferentially be stronger beamed. In unified schemes for AGN (e.g., Urry & Padovani 1995), flat-spectrum radio quasars (FSRQ) are objects whose radio and optical continuum emission is enhanced by relativistically beamed emission from a jet; hence, part of the X-ray emission will also be enhanced by beaming. However, the “blazar sequence” (Fossati et al. 1998) appears to indicate that beamed X-ray emission is progressively less important in objects with higher optical (accretion disc) luminosity (although a number of recent authors have questioned the reality of the blazar sequence; e.g., Antón & Browne 2005; Landt et al. 2006; Nieppola et al. 2006). Based on correlations between X-ray, radio and optical fluxes, a number of authors concluded already in the *Einstein* era that there has to be a beamed component of X-ray emission in sources with beamed radio emission (Kembhavi et al. 1986; Browne & Murphy 1987; Shastri 1991; Shastri et al. 1993; Jackson et al. 1993; Kembhavi 1993). Later, Baker et al. (1995) found a beaming-induced correlation between radio and X-ray fluxes both for steep-spectrum and flat-spectrum quasars, while both Galbiati et al. (2005) and Grandi et al. (2006) report evidence for a beamed contribution in FSRQ, but not in other radio-loud quasars. On the other hand, Evans et al. (2006) found a contribution to the X-ray emission of high-power radio galaxies and quasars from *both* the accretion flow (i.e., the disc) and the jet, indicating that the X-ray emission is not *purely* due to a beamed component.

To consider whether beaming is important in the optical, we begin with the observation that the  $H\alpha$  equivalent width of *all* types of AGN is essentially constant (Osterbrock 1989, Fig. 11.6) and independent of the radio properties (see also Boroson & Green 1992, §4.2; this statement is *not* contradicted by the anticorrelation between continuum luminosity and equivalent width of quasar emission lines known as the Baldwin effect [Baldwin 1977], as that effect is strongest in high-ionization lines like  $Ly\alpha$  and C IV). The constant Balmer-line width implies that beaming does not change the optical continuum luminosity significantly. Hence, we expect FSRQs to have much higher values of  $R$  than other AGN purely due to relativistic beaming. At the same time, these objects may have also a high non-thermal fraction due to beaming of the X-ray emission. Hence, the trend for radio-loud sources to be found at higher values of the non-thermal fraction may be due to relativistic beam-

ing affecting radio and X-ray emission, but not the optical emission, in sources with the most powerful relativistic jets (the trend of average  $R$  increasing to the right in Fig. 2). Unfortunately, we do not have spectral information for our radio sources, so that we cannot remove the FSRQ from our plot and check whether the remaining radio-loud objects still show the same trend.

Nevertheless, it appears unlikely that the observed trends are exclusively due to beaming and not connected to some intrinsic differences. First, the trend for the average  $R$  to increase with higher *total* luminosity cannot be caused exclusively by beaming, as there are high- $R$  objects whose total luminosity is more than 50% optical (thermal disc) emission. Secondly, the radio-quiet and radio-loud quasar population cannot be unified using orientation and beaming alone (see Kellermann et al. 1989 and references therein; Rawlings & Saunders 1991; Miller et al. 1993). In other words, there is an intrinsic difference in addition to relativistic beaming that gives some sources a much higher  $R$  value than most others. We verified that the observed gradient in average radio loudness on the DFLD is also visible if we plot the fraction of radio loud objects ( $R > 10$ ) on the DFLD. Third, there is no correlation between the radio and X-ray fluxes for the objects in our SDSS sample, unlike in the samples considered by Galbiati et al. (2005) and Grandi et al. (2006). Hence, even with a beamed contribution to the X-rays, the fact that sources with high thermal fraction are also more likely to have a high  $R$  value also has to arise from an intrinsic connection between thermal fraction and  $R$  other than relativistic beaming.

In our analysis we use a fixed hydrogen column density for all quasars. The used ROSAT fluxes are sensitive to changes in the column density. Thus, strong variations in the intrinsic column density of the quasars may change the position of the sources on the DFLD. However, the majority of our sources is at moderate redshifts ( $z \sim 1$ ) so the observed photons have been emitted as harder X-rays and are less sensitive to intrinsic obscuration. All our SDSS quasars have broad lines. According to the “standard unification” of AGN, the intrinsic column density is small or negligible in these broad line sources (for absorption see Richards et al. 2003, e.g., for the column density Granato et al. 1997, e.g.). Nevertheless, we cannot rule out completely that absorption affects our DFLD. However, for this to become the dominant effect, there would have to be a strong anticorrelation between radio loudness and hydrogen column density, which we consider to be unlikely given that all objects in the sample are broad-line objects and selected on optical continuum magnitude.

Finally, neglecting the contribution of host galaxy starlight to the SDSS optical quasar magnitudes has the tendency to let lower-luminosity and lower-redshift sources appear too optically luminous. Furthermore, it artificially increases the disc fraction and lowers the  $R$  value. However, Vanden Berk et al. (2006) have performed a spectral decomposition of SDSS quasar spectra and find that only 20% of the objects considered have a host galaxy fraction of more than 50%, and hardly any have a host galaxy fraction of more than 90%. Thus, the host galaxy contribution affects only a small fraction of objects, and only in the lower left-hand part of the DFLD. They will not affect the high-luminosity sources that create most of the signal in the upper

right-hand part of the DFLD. Nevertheless, it would clearly be desirable to repeat our experiment including host galaxy corrections.

#### 4.4 Size-luminosity evolution of radio sources

We only have radio data at a single observing frequency, 1.4 GHz, and with a rather large beam size of  $5''$ , corresponding to physical scales between 17 kpc at  $z = 0.2$ , our low-redshift cutoff, and 42 kpc at  $z = 1.6$ , where the angular diameter distance is maximal for our chosen cosmology. This implies that there will be some contribution to our “core” luminosities from extended lobe components in the FIRST beam. This is not a problem for sources which are large enough for the lobes to be clearly separated from the core in FIRST imaging, since the SDSS catalog matching employs a rather small matching radius ( $3''$ ) for FIRST sources. However, Kaiser et al. (1997) have shown that lobes are more luminous when the source is smallest, exacerbating the problem for sources where the core cannot be discerned from the lobes based on the FIRST imaging. Nevertheless, these sources have lobes precisely *because* they have powerful jets, so that they must have a large core radio flux, too. Hence, any contribution from unresolved lobes will have the effect of increasing the inferred value of  $R$  only in sources that have a high radio loudness anyway, but it will not increase the radio loudness of sources without a jet. In other words, lobe contamination makes radio-loud sources even more radio-loud, but it does not create false positives in regions of the DFLD where there are no radio-loud sources.

## 5 DISCUSSION: ANALOGIES WITH XRBs

We have shown in the previous section that quasars are more likely to be radio-loud if the X-ray luminosity is large compared to the thermal disc luminosity and/or the source is very luminous. This suggests the radio loudness depends at least on 2 parameters: the total accretion rate as well as a measure of the relative prominence of the non-thermal X-ray component compared to the thermal disc emission. This effect is similar to that observed in XRBs, which motivated our development of the DFLD. Here we compare the behaviour of AGN with XRBs.

### 5.1 Monte-Carlo simulation of an XRB population DFLD

For X-ray binaries, we can study the evolution of single objects in the HID during their outbursts (e.g., Fig. 11), while we have to consider AGN as a population. Nevertheless, as DFLDs are constructed as an analogue of the HIDs, the overall distribution of a population of XRBs in an HID and the distribution of our AGN sample in a DFLD should be similar. Indeed, XRBs and AGN populate the right side of their diagrams at low luminosities and create a cloud of objects in the soft and IM states further to the left at higher luminosities (Fender et al. 2004). To compare XRBs and AGN in more detail, we simulate a DFLD for an XRB population of 100 objects based on our knowledge of the evolution of the disc and the power law component in an outburst cycle of an XRB (a sufficient number of observed HIDs is not

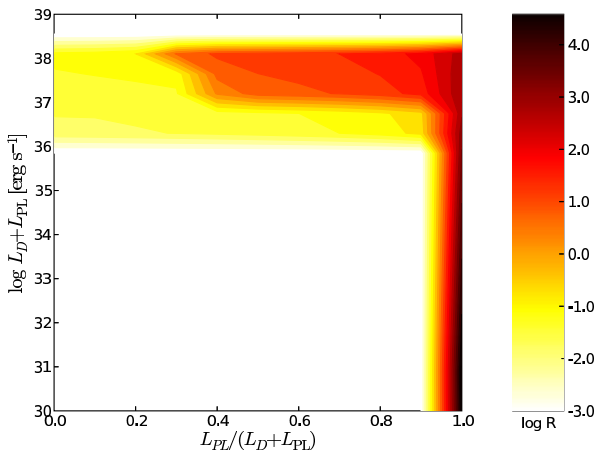


**Figure 10.** DFLD for a simulated sample of XRBs. We simulated 100 outbursts of an XRB.

readily accessible to us). We fix the black-hole mass of the simulated XRBs at  $10M_{\odot}$  (see e.g., Orosz 2003).

For each simulated outburst, we first choose the accretion rate at the hard-to-soft state transition  $\dot{M}_{\text{crit}}$  randomly from the range 5%-100% Eddington. We use  $L_R/L_D$  as measure of the radio loudness to retain the same physical meaning as  $L_R/L_O$  for AGN. During its outburst the source moves through its canonical states, and we compute luminosities for each of the source components using the prescription given in Appendix B.

Figure 10 shows the simulated DFLD for 100 XRB outbursts. The overall distribution of the simulated XRBs in the DFLD is similar to the observed diagram for AGN. Also the radio loudness distribution is similar for XRBs and AGN. The sources at the right-hand edge of the diagram are the most radio-loud objects. In the upper part, where the SDSS quasars are located in the AGN DFLD, we find a gradient from high average  $R$  in top right-hand corner to a low average  $R$  in the bottom left part, both for the simulated XRBs and the observed AGN. For XRBs, the jet is quenched (we assumed quenching by a factor 100) in the bottom left corner of the upper part of the diagram (Fig. 2); by contrast, all sources in the top right-hand corner are extremely radio-loud. The gradient in radio loudness is smaller for AGN, and we will discuss possible reasons below. At low luminosities, both XRBs and AGN are located in the right/power-law dominated side of the diagram.

## 5.2 Further evidence for common accretion states in XRBs and AGN

The similarity of the DFLDs of XRBs and AGN further supports the idea that AGN have the same accretion states as XRBs. In both classes of object, the hard state is characterized by the absence of a strong disc component, a power-law component dominating the total luminosity, and the presence of a jet. The jet power is likely to dominate over the radiated power (Körding et al. 2006). In the AGN zoo, we classify LLAGN and FR I radio galaxies as hard state objects, (as already suggested by Meier 2001; Falcke et al. 2004; Maccarone et al. 2003; Ho 2005; Körding et al. 2006).

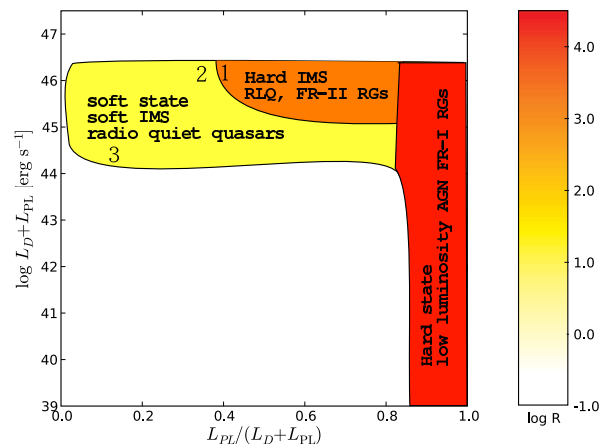


**Figure 11.** Sketch of the distribution AGN and XRB states (scaled to AGN masses) on the DFLD. As discussed in the text, a lobe-dominated AGN could undergo a strong change in the core properties, moving it from position “1” to position “2”, but the corresponding change in the lobe properties would be delayed by at least the fading time of the lobe, so that it would appear to be too radio-loud based on FIRST data. By contrast, AGN at position “3” should have no lobes.

The hard IMS has some disc contribution, but the radio jet is still active (Fender et al. 2004). In the AGN population, we suggest that this state corresponds to the radio-loud quasars. In the soft IMS and the soft state in XRBs which are even more disc-dominated, the jet is not observable in the radio. The corresponding AGN class are the radio quiet quasars. In Fig. 11 we show a schematic diagram of the distribution of the states in our DFLD.

For XRBs each cell of the DFLD can be associated with a given class, as we have assumed that the BH masses of XRBs are similar and used a deterministic evolution for all sources. Therefore, we find a fast transition in our simulation from the radio-loud hard state and hard IMS to the radio-quiet states (soft and soft IMS). In our AGN sample, we have a large BH mass range and orientation will affect the observed luminosities. Thus, the sharp transitions will be washed out. Even if a cell was associated, for example, with the hard IMS, there would still be a fraction of radio-quiet sources in this bin due to different BH masses or source peculiarities.

With long radio observations, it is usually possible to find radio emission from all radio-quiet quasars, and there are correlations between radio and emission-line luminosity both for radio-quiet and radio-loud objects (e.g., Miller et al. 1993; Falcke et al. 1995; Xu et al. 1999; Ho & Peng 2001). The difference in radio loudness between radio-loud and quiet quasars is typically around a factor 100 (e.g., Kellermann et al. 1989). For XRBs it is often stated that the radio jet is quenched (e.g., Fender et al. 1999) in the soft state. However, the upper limits on the radio flux on high state objects are not yet low enough to rule out radio emission from “quenched” XRBs at a level equivalent to that in radio-quiet quasars (one of the best studied cases is XTE J1550–564 where Corbel et al. (2001) find that the radio emission is quenched by at least a factor 50). The anal-

ogy between XRBs and AGN therefore suggests that very deep radio observations of soft-state XRBs should detect radio emission.

For XRBs we can measure how fast a source moves through the DFLD. For AGN it is not yet known how long a source spends in each accretion state. State changes in AGN might be triggered by the same process as in XRBs, e.g., disc instabilities (cf., Frank et al. 2002). But already different XRBs or different outbursts of the same source move through the diagram at different speeds. Furthermore, environmental effects can also change the external accretion rate dramatically (e.g. during a galaxy merger), thus the timescales do not have to scale linearly with black hole mass. These timescales will not play an important role for the radio luminosity as a function of the position in the DFLD as long as the radio emission responds to changes in the accretion rate on a faster timescale than the timescale of a state change. Our radio data is from the FIRST survey, i.e., high-angular resolution images at 1.4 GHz. Especially at higher redshifts the corresponding emitted frequency is even higher and the radio emission is likely to originate predominantly from the radio core. The emission region is therefore fairly small (parsec-scale) and the radio flux will respond to any state changes rather quickly ( $\sim$  a few years) — similar to XRB case (here the response is even faster,  $\sim$  hours). However, the large-scale radio structure (radio lobes) responds much more slowly. It is therefore likely that some sources changing from the radio-loud hard intermediate state to the radio-quiet soft state still have strong radio lobes, even though the core is already in a radio-quiet state. For a 100-kpc quasar jet, we see the core change up to 200 ky *earlier* than the near lobe. The importance of this delay depends on the sum of the fading time of the lobe and the typical lag between the time when *we* see the core properties change, and the time when the *lobe* receives the information that the core properties have changed. On the DFLD in Fig. 11 we have marked three positions with the numbers 1 to 3. In the area marked as “1” we expect to observe predominantly sources in the hard intermediate state, i.e., sources with an active radio core and possibly strong radio lobes. Some sources in the area “2” may have just changed their accretion state to the soft state. Thus, some sources should have a weak radio core but still have strong radio lobes. In comparison, area “3” should be populated mainly with sources with no lobes and only weak radio cores.

### 5.3 Other DFLD trends: timing and jet Lorentz factor

In XRBs, there are correlations between the source’s position in the DFLD and other observables than just the radio loudness. Looking for their presence in AGN will be a strong test of the AGN-XRB unification scenario.

The timing features of XRBs depend on the accretion state of the object and therefore on its position in the DFLD. Hard-state objects on the right side of the diagram show strong flat-topped band limited noise (see van der Klis 2006). Soft-state objects on the lower left part of the DFLD (area “3” in Fig. 11) should mainly show weak power-law noise. During the IMS strong quasi-periodic oscillations (QPOs) are found. Near the transition from the hard to the soft IMS, objects often show strong QPOs around 6 Hz (type

B; Wijnands et al. 1999; Belloni et al. 2005). With a linear mass scaling, this would translate into a period of  $\sim$  200 d for objects in area “1” and “2”. However, as with the radio loudness map, different black-hole masses and source peculiarities (obscuration, beaming) will “smear out” the sources in the DFLD, so there will not be a sharp transition as found in a single XRB outburst.

Also the bulk Lorentz factor of XRB jets may depend on the position in the DFLD (Fender et al. 2004). It would be interesting to see if this is also the case for AGN. To do so, one would need a large sample of AGN with a measure of their bulk Lorentz factors. However, reliable measurements of Lorentz factors are hard to obtain (Fender 2003). If we approach the jet line in the DFLD, the jet in XRBs become unstable and one observes rapid ejections (Fender et al. 2004). It is not yet clear whether this behaviour is also found in AGN. One caveat is that while hard-state XRBs seem to have rather slow jets, it is thought that those in BL Lac objects are highly relativistic. According to the orientation unification schema of AGN, the parent population of BL Lac objects are low-luminosity FR I radio galaxies, which are likely to be hard state objects. Thus, it may be that the jet velocities are different for stellar and supermassive black holes or that the observed slow jets have a fast spine that has not yet been observed in XRBs. A detailed study is needed to decide whether the speeds of AGN jets are similar to those of XRB jets.

## 6 CONCLUSIONS

We have shown that the hardness-intensity diagrams used to diagnose the states of XRBs can be generalised to disc-fraction/luminosity diagrams (DFLDs), which can be used both for AGN and XRBs. The shape of the distribution of low-luminosity AGN and SDSS quasars in this diagram is similar to that of XRBs. Additionally, supermassive and stellar-mass black holes show a similar dependence of radio loudness on position in the DFLD. This suggests that radio loudness can only be understood in context of a two-dimensional diagram, i.e., as function of non-thermal fraction and luminosity, and is not directly related to a single variable like the accretion rate or black-hole mass. The similarity of the diagrams for AGN and XRBs supports the idea that AGN have the same accretion states as XRBs.

At low luminosities, AGN and XRBs are always in their hard state, which is characterized by strong X-ray and radio emission compared to their disc emission. At higher luminosities, AGN can either be in their radio-loud hard IMS (radio-loud quasars) or their soft state or soft IMS (radio-quiet quasar). The position of an AGN in the DFLD determines the probability with which it is in each of these states. Thus, we find the same coupling between accretion flow/disc and jet properties in AGN as in X-ray binaries.

To avoid all evolutionary and selection effects, it will be desirable to repeat our investigation with a sample of AGN from a single narrow redshift range, but with high dynamic range in luminosity and well-determined masses. Ideally, the sample would extend down to LLAGN, which can to date only be found in the nearby universe, but not in the same volume as large numbers of quasars. Further strong tests of the AGN-XRB unification and our proposed equivalence

between XRB states and members of the AGN zoo will be performed by looking for correlations between DFLD position and other properties, such as QPO frequencies.

## ACKNOWLEDGEMENTS

The authors thank Tom Maccarone for helpful discussions. SJ was supported by the Max-Planck-Institut für Astronomie through an Otto Hahn Fellowship. We thank our referee for constructive comments.

Funding for the Sloan Digital Sky Survey<sup>4</sup> (SDSS) has been provided by the Alfred P. Sloan Foundation, the Participating Institutions, the National Aeronautics and Space Administration, the National Science Foundation, the U.S. Department of Energy, the Japanese Monbukagakusho, and the Max Planck Society. The SDSS is managed by the Astrophysical Research Consortium (ARC) for the Participating Institutions. The Participating Institutions are The University of Chicago, Fermilab, the Institute for Advanced Study, the Japan Participation Group, The Johns Hopkins University, the Korean Scientist Group, Los Alamos National Laboratory, the Max-Planck-Institute for Astronomy (MPIA), the Max-Planck-Institute for Astrophysics (MPA), New Mexico State University, University of Pittsburgh, University of Portsmouth, Princeton University, the United States Naval Observatory, and the University of Washington.

## REFERENCES

- Abazajian K., Adelman-McCarthy J. K., Agüeros M. A., Allam S. S., Anderson S. F., Annis J., Bahcall N. A., Baldry I. K., et al., 2003, *AJ*, 126, 2081
- Abramowicz M. A., Kluźniak W., McClintock J. E., Remillard R. A., 2004, *ApJ*, 609, L63
- Adelman-McCarthy J. K., Agüeros M. A., Allam S. S., Anderson K. S. J., Anderson S. F., Annis J., Bahcall N. A., Baldry I. K., Barentine J. C., Berlind A., Bernardi M., Blanton M. R., Boroski W. N., et al., 2006, *ApJS*, 162, 38
- Anderson S. F., Voges W., Margon B., Trümper J., Agüeros M. A., Boller T., Collinge M. J., Homer L., et al., 2003, *AJ*, 126, 2209
- Antón S., Browne I. W. A., 2005, *MNRAS*, 356, 225
- Antonucci R., 1993, *ARA&A*, 31, 473
- Baker J. C., Hunstead R. W., Brinkmann W., 1995, *MNRAS*, 277, 553
- Baldwin J. A., 1977, *ApJ*, 214, 679
- Barcons X., Carrera F. J., Watson M. G., McMahon R. G., Aschenbach B., Freyberg M. J., Page K., Page M. J., Roberts T. P., Turner M. J. L., Barret D., et al., 2002, *A&A*, 382, 522
- Belloni T., Homan J., Casella P., van der Klis M., Nespole E., Lewin W. H. G., Miller J. M., Méndez M., 2005, *A&A*, 440, 207
- Blandford R. D., Königl A., 1979, *ApJ*, 232, 34
- Boroson T. A., 2002, *ApJ*, 565, 78
- Boroson T. A., Green R. F., 1992, *ApJS*, 80, 109
- Browne I. W. A., Murphy D. W., 1987, *MNRAS*, 226, 601
- Chen W., Shrader C. R., Livio M., 1997, *ApJ*, 491, 312
- Chen X., Abramowicz M. A., Lasota J.-P., Narayan R., Yi I., 1995, *ApJ*, 443, L61
- Corbel S., Fender R. P., Tzioumis A. K., Nowak M., McIntyre V., Durouchoux P., Sood R., 2000, *A&A*, 359, 251
- Corbel S., Kaaret P., Jain R. K., Bailyn C. D., Fender R. P., Tomsick J. A., Kalemci E., McIntyre V., Campbell-Wilson D., Miller J. M., McCollough M. L., 2001, *ApJ*, 554, 43
- Dickey J. M., Lockman F. J., 1990, *ARA&A*, 28, 215
- Elvis M., Wilkes B. J., McDowell J. C., Green R. F., Bechtold J., Willner S. P., Oey M. S., Polonski E., Cutri R., 1994, *ApJS*, 95, 1
- Esin A. A., McClintock J. E., Narayan R., 1997, *ApJ*, 489, 865+
- Evans D. A., Worrall D. M., Hardcastle M. J., Kraft R. P., Birkinshaw M., 2006, *ApJ*, 642, 96
- Falcke H., Biermann P. L., 1995, *A&A*, 293, 665
- Falcke H., Körding E., Markoff S., 2004, *A&A*, 414, 895
- Falcke H., Malkan M. A., Biermann P. L., 1995, *A&A*, 298, 375
- Fender R., Corbel S., Tzioumis T., McIntyre V., Campbell-Wilson D., Nowak M., Sood R., Hunstead R., Harmon A., Durouchoux P., Heindl W., 1999, *ApJ*, 519, L165
- Fender R. P., 2001, *MNRAS*, 322, 31
- Fender R. P., 2003, *MNRAS*, 340, 1353
- Fender R. P., Belloni T. M., Gallo E., 2004, *MNRAS*, 355, 1105
- Fossati G., Maraschi L., Celotti A., Comastri A., Ghisellini G., 1998, *MNRAS*, 299, 433
- Franceschini A., Vercellone S., Fabian A. C., 1998, *MNRAS*, 297, 817
- Frank J., King A., Raine D. J., 2002, *Accretion Power in Astrophysics: Third Edition. Accretion Power in Astrophysics*, by Juhan Frank and Andrew King and Derek Raine, pp. 398. ISBN 0521620538. Cambridge, UK: Cambridge University Press, February 2002.
- Galbiati E., Caccianiga A., Maccacaro T., Braito V., Della Ceca R., Severgnini P., Brunner H., Lehmann I., Page M. J., 2005, *A&A*, 430, 927
- Granato G. L., Danese L., Franceschini A., 1997, *ApJ*, 486, 147
- Grandi P., Malaguti G., Fiocchi M., 2006, *ApJ*, 642, 113
- Ho L. C., 1999, *ApJ*, 516, 672
- Ho L. C., 2002, *ApJ*, 564, 120
- Ho L. C., 2005, *Ap&SS*, 300, 219
- Ho L. C., Filippenko A. V., Sargent W. L. W., 1997, *ApJS*, 112, 315
- Ho L. C., Peng C. Y., 2001, *ApJ*, 555, 650
- Hogg D. W., Baldry I. K., Blanton M. R., Eisenstein D. J., 2002, *ArXiv Astrophysics e-prints*
- Homan J., Wijnands R., van der Klis M., Belloni T., van Paradijs J., Klein-Wolt M., Fender R., Méndez M., 2001, *ApJS*, 132, 377
- Hopkins P. F., Strauss M. A., Hall P. B., Richards G. T., Cooper A. S., Schneider D. P., Vanden Berk D. E., Jester S., Brinkmann J., Szokoly G. P., 2004, *AJ*, 128, 1112
- Ivezić Ž., Menou K., Knapp G. R., Strauss M. A., Lupton R. H., Vanden Berk D. E., Richards G. T., Tremonti C., et al., 2002, *AJ*, 124, 2364
- Jackson N., Browne I. W. A., Warwick R. S., 1993, *A&A*, 274, 79
- Jarvis M. J., McLure R. J., 2002, *MNRAS*, 336, L38

<sup>4</sup> <http://www.sdss.org>

- Jester S., 2005, *ApJ*, 625, 667
- Kaiser C. R., Dennett-Thorpe J., Alexander P., 1997, *MNRAS*, 292, 723
- Kellermann K. I., Sramek R., Schmidt M., Shaffer D. B., Green R., 1989, *AJ*, 98, 1195
- Kembhavi A., 1993, *MNRAS*, 264, 683
- Kembhavi A., Feigelson E. D., Singh K. P., 1986, *MNRAS*, 220, 51
- K rding E., Falcke H., 2004, *A&A*, 414, 795
- K rding E. G., Falcke H., Corbel S., 2006, astro-ph/0603117, Accepted for publication in *A&A*2006
- K rding E. G., Fender R. P., Migliari S., 2006, *MNRAS*, 369, 1451
- Lacy M., Laurent-Muehleisen S. A., Ridgway S. E., Becker R. H., White R. L., 2001, *ApJ*, 551, L17
- Landt H., Perlman E. S., Padovani P., 2006, *ApJ*, 637, 183
- Laor A., 2000, *ApJ*, 543, L111
- Maccarone T. J., Gallo E., Fender R., 2003, *MNRAS*, 345, L19
- Markoff S., Falcke H., Fender R., 2001, *A&A*, 372, L25
- Markoff S., Nowak M., Wilms J., 2005, *ApJ*, 635, 1203
- Markowitz A., Edelson R., Vaughan S., Uttley P., George I. M., Griffiths R. E., Kaspi S., Lawrence A., McHardy I., Nandra K., Pounds K., Reeves J., Schurch N., Warwick R., 2003, *ApJ*, 593, 96
- McLure R. J., Dunlop J. S., 2004, *MNRAS*, 352, 1390
- McLure R. J., Jarvis M. J., 2004, *MNRAS*, 353, L45
- Meier D. L., 2001, *ApJ*, 548, L9
- Merloni A., Heinz S., Di Matteo T., 2003, *MNRAS*, 345, 1057
- Merritt D., Ferrarese L., 2001, *ApJ*, 547, 140
- Miller J. M., Homan J., Steeghs D., Rupen M., Hunstead R. W., Wijnands R., Charles P. A., Fabian A. C., 2006, astro-ph/0602633 e-prints
- Miller P., Rawlings S., Saunders R., 1993, *MNRAS*, 263, 425
- Mirabel I. F., Rodr guez L. F., 1999, *ARA&A*, 37, 409
- Nagar N. M., Falcke H., Wilson A. S., 2005, *A&A*, 435, 521
- Narayan R., Yi I., 1994, *ApJ*, 428, L13
- Nieppola E., Tornikoski M., Valtaoja E., 2006, *A&A*, 445, 441
- Nowak M. A., 1995, *PASP*, 107, 1207+
- Oke J. B., Gunn J. E., 1983, *ApJ*, 266, 713
- Orosz J. A., 2003, in *IAU Symposium Inventory of black hole binaries*. pp 365–
- Osterbrock D. E., 1989, *Astrophysics of gaseous nebulae and active galactic nuclei*. University Science Books, Mill Valley, CA
- Pounds K. A., Done C., Osborne J. P., 1995, *MNRAS*, 277, L5
- Prugniel P., Zasov A., Busarello G., Simien F., 1998, *A&AS*, 127, 117
- Ptak A., Griffiths R., 2003, in *ASP Conf. Ser. 295: Astronomical Data Analysis Software and Systems XII XASist: A System for the Automation of X-ray Astrophysics Analysis*. pp 465–
- Rawlings S., Saunders R., 1991, *Nature*, 349, 138
- Remillard R. A., 2005, *ArXiv Astrophysics e-prints*
- Richards G. T., 2006, *ArXiv Astrophysics e-prints*
- Richards G. T., Fan X., Newberg H. J., Strauss M. A., Vanden Berk D. E., Schneider D. P., Yanny B., Boucher A., et al., 2002, *AJ*, 123, 2945
- Richards G. T., Hall P. B., Vanden Berk D. E., Strauss M. A., Schneider D. P., Weinstein M. A., Reichard T. A., York D. G., Knapp G. R., Fan X., Ivezi  Z., Brinkmann J., Budav ri T., Csabai I., Nichol R. C., 2003, *AJ*, 126, 1131
- Richards G. T., Strauss M. A., Fan X., Hall P. B., Jester S., Schneider D. P., Vanden Berk D. E., for the SDSS Collaboration 2006, *ArXiv Astrophysics e-prints*
- ROSAT Scientific Team 2000, *VizieR Online Data Catalog*, 9028, 0
- Shakura N. I., Sunyaev R. A., 1973, *A&A*, 24, 337
- Shastri P., 1991, *MNRAS*, 249, 640
- Shastri P., Wilkes B. J., Elvis M., McDowell J., 1993, *ApJ*, 410, 29
- Shen S., White S. D. M., Mo H. J., Voges W., Kauffmann G., Tremonti C., Anderson S. F., 2006, *MNRAS*, pp 582–+
- Sunyaev R. A., Tr mper J., 1979, *Nature*, 279, 506
- Tananbaum H., Gursky H., Kellogg E., Giacconi R., Jones C., 1972, *ApJ*, 177, L5
- Terashima Y., Wilson A. S., 2003, *ApJ*, 583, 145
- Thorne K. S., Price R. H., 1975, *ApJ*, 195, L101
- Ueda Y., Akiyama M., Ohta K., Miyaji T., 2003, *ApJ*, 598, 886
- Urry C. M., Padovani P., 1995, *PASP*, 107, 803
- Uttley P., McHardy I. M., Papadakis I. E., 2002, *MNRAS*, 332, 231
- van der Klis M., 2006, *Compact Stellar X-Ray Sources*, eds. W.H.G. Lewin and M. van der Klis, Cambridge University Press, in press (astro-ph/0410551)
- Vanden Berk D. E., Shen J., Yip C.-W., Schneider D. P., Connolly A. J., Burton R. E., Jester S., Hall P. B., Szalay A. S., Brinkmann J., 2006, *AJ*, 131, 84
- Vestergaard M., 2004, in Richards G. T., Hall P. B., eds, *ASP Conf. Ser. 311: AGN Physics with the Sloan Digital Sky Survey Black-Hole Mass Measurements*. pp 69–+
- Voges W., Aschenbach B., Boller T., Br uning H., Briel U., Burkert W., Dennerl K., Englhauser J., Gruber R., Haberl F., Hartner G., Hasinger G., et al., 1999, *A&A*, 349, 389
- White R. L., Becker R. H., Helfand D. J., Gregg M. D., 1997, *ApJ*, 475, 479
- Wijnands R., Homan J., van der Klis M., 1999, *ApJ*, 526, L33
- Willott C. J., Rawlings S., Blundell K. M., Lacy M., Eales S. A., 2001, *MNRAS*, 322, 536
- Woo J., Urry C. M., 2002, *ApJ*, 581, L5
- Woo J.-H., Urry C. M., van der Marel R. P., Lira P., Maza J., 2005, *ApJ*, 631, 762
- Xu C., Livio M., Baum S., 1999, *AJ*, 118, 1169
- Zamorani G., Henry J. P., Maccacaro T., Tananbaum H., Soltan A., Avni Y., Liebert J., Stocke J., Strittmatter P. A., Weymann R. J., Smith M. G., Condon J. J., 1981, *ApJ*, 245, 357
- Zdziarski A. A., Johnson W. N., Done C., Smith D., McNaron-Brown K., 1995, *ApJ*, 438, L63
- Zhang S. N., Cui W., Harmon B. A., Paciesas W. S., Remillard R. E., van Paradijs J., 1997, *ApJ*, 477, L95

## APPENDIX A: SQL QUERY FOR SDSS QUASAR SAMPLE

The query selects all objects from the SDSS spectroscopic database that are classified with high confidence as a quasar, and, where available, ROSAT and FIRST parameters.

```
select ...
from specphoto as sp
left outer join rosat as ro on ro.objid = sp.objid
left outer join first as fi on sp.objid = fi.objid
where specclass in (3,4)
and zconf >= 0.35
and z between 0.2 and 2.5
```

## APPENDIX B: RECIPE FOR SIMULATING AN XRB OUTBURST CYCLE

Here, we describe our assumptions on the evolution of an XRB during a single outburst. A source is assumed to be in quiescence before the start of the simulation, i.e., we start the simulation with the rise of the outburst.

- Initial hard state: When a source starts its outburst, it is in the hard state with its SED dominated by the power law component. Therefore, we set  $L_{\text{PL}} = \left(\frac{\dot{M}}{\dot{M}_{\text{crit}}}\right)^2 0.1\dot{M}_{\text{crit}}c^2$ , assuming a quadratic scaling of the luminosity with accretion rate as expected for inefficient flow or jet models (theoretical prediction: Narayan & Yi 1994, empirical: K rding et al. 2006). The jet is active and the radio luminosity  $L_{\text{R}} \propto \dot{M}^{1.4}$  (Blandford & Konigl 1979; Falcke & Biermann 1995). The disc is usually not directly visible in this state, we set its luminosity to 1 % of the PL component.

- IMS: During the transition, the bolometric luminosity does not change significantly (Zhang et al. 1997). Thus, we set  $L_{\text{PL}} = (1 - \xi) \times 0.1\dot{M}_{\text{crit}}c^2$  and  $L_{\text{D}} = \xi \times 0.1\dot{M}_{\text{crit}}c^2$ , where  $\xi$  is the disc fraction during the transition. The radio jet is active up to the jet line (Fender et al. 2004), which may vary with the critical accretion rate  $\dot{M}_{\text{crit}}$ . Higher-luminosity outbursts have an active jet up to larger disc fractions  $\xi$ . We set the jet line at  $\xi = 0.57 + \frac{\dot{M}_{\text{crit}}c^2}{10^{36} \text{ erg s}^{-1}}$ , which is normalised for the transition in GX 339-4 observed by Belloni et al. (2005). The jet power up to the jet line is assumed to be constant and equal to the maximum jet power achieved in the hard state (i.e., both the radiative and the kinetic luminosity remain constant during the transition). We omit the relativistic ejections which happen right at the transition to the radio-quiet phase, as they are very short-lived. Their inclusion would yield a higher radio flux right at the jet line. The strength and size on the DFLD of this feature depends on the timescales of a source moving on the DFLD compared to the timescale of a responds in the radio (see discussion in sec. 5.2).

- In the soft state, the SED is dominated by the soft-spectrum, efficiently radiating accretion disc:  $L_{\text{D}} = 0.1\dot{M}c^2$ . A hard power law is often visible up to very high photon energies, we assume  $L_{\text{PL}} = 0.01L_{\text{D}}$ . The radio jet is quenched by a factor 100 compared to the hard state.

- IMS: The transition back towards the hard state happens at lower luminosity than the hard-to-soft transition. The hysteresis is smaller for smaller transition luminosities;

Cyg X-1, e.g., is nearly always near the transition and does not show any hysteresis. Thus, we set  $\log(0.1\dot{M}_{\text{back}}c^2) = 37 - 0.5(\log(0.1\dot{M}_{\text{crit}}c^2) - 37)$ , where all luminosities are measured in  $\text{erg s}^{-1}$ . For this transition we use a similar prescription for the power-law luminosity as in the first transition:  $L_{\text{PL}} = (1 - \xi) 0.1\dot{M}_{\text{back}}c^2$  and  $L_{\text{D}} = \xi 0.1\dot{M}_{\text{back}}c^2$ , but the jet is assumed to be quenched during the whole transition and is expected to restart only when the source enters its hard state.

- Declining hard state: same as initial hard state, just  $\dot{M}_{\text{crit}}$  is exchanged with  $\dot{M}_{\text{back}}$